Comparative Theoretical Study of Rotamerism and Excited State Intramolecular Proton Transfer of 2-(2′-Hydroxyphenyl)benzimidazole, 2-(2′-Hydroxyphenyl)imidazo[4,5-b]pyridine, 2-(2′-Hydroxyphenyl)imidazo[4,5-c] pyridine and 8-(2′-Hydroxyphenyl)purine

Francis A. S. Chipem and G. Krishnamoorthy*

Department of Chemistry, Indian Institute of Technology Guwahati, Guwahati 781039, India

Received: April 17, 2009; Revised Manuscript Received: September 8, 2009

The effect of nitrogen substitution in the benzene ring of 2-(2′-hydroxyphenyl)benzimidazole (HPBI) on the photophysics and rotamerization were examined theoretically by a comparative study of HPBI with 2-(2′-hydroxyphenyl)imidazo[4,5-b]pyridine (HPIP-b), 2-(2′-hydroxyphenyl)imidazo[4,5-c]pyridine (HPIP-c), and 8-(2′-hydroxyphenyl)purine (HPP). Density functional theory (DFT) was used for ground state calculations. Restricted configuration interaction singles (RCIS) combined time dependent DFT (TDDFT) was used for excited state calculations. The calculations reveal in the ground state all of the molecules have two stable rotameric forms, but their relative population is strongly affected by nitrogen substitution. The excitation and emission bands have been calculated theoretically for the rotamers and tautomers. Fluorescence emission and excitation spectra were recorded for HPBI in dioxane and compared with the theoretical results. Theoretical excitation and emission data are in good agreement with the available experimental data. The potential energy surface simulated for the proton transfer processes reflect that it is not favorable in S_0 state, but it is feasible in S_1 state in all of the molecules. Except in HPIP-b, HPIP-b′, and HPP′, in all other nitrogen substituted molecules, the energy difference between the keto and enol form along the excited state proton transfer coordinates decreases compared to that in HPBI. The study also reveals that torsional relaxation of tautomer to twisted state competes with radiative transitions and leads to fluorescence quenching. Nitrogen substitution enhances this torsional induced nonradiative process and it follows the order HPBI < HPIP-b < HPIP-c < HPP.

1. Introduction

Photo induced electron transfer and proton transfer are fundamental processes that occur in a number of natural systems. Tremendous interest has been shown by the photochemists and photophysicists in studying photoinduced proton transfer process in general[1,2] and excited state intramolecular proton transfer (ESIPT)[3,4] in particular, owing to the simplicity and fundamental importance of its reaction pattern. ESIPT process involves the presence of intramolecular hydrogen bond between the acidic group and the basic group that are in close proximity in the ground state. Upon excitation to the first excited state, the acidity of the acidic center and the basicity of the basic center increase because of a change in charge density. This leads to migration of proton along the hydrogen bond coordinate to give phototautomer. ESIPT is generally extensively fast occurring within subpicosecond time scale, and on excitation the molecule passes to the potential well of the tautomeric species almost instantaneously and then relaxes vibrationally.[5,6] Usually ESIPT active molecules show dual emission, one being the normal emission from the local excitation and the other which is largely Stokes-shifted as high as 10 000 cm^{-1}, due to the tautomer formed by proton transfer. The characteristics of normal and the tautomer emissions and subsequently their ratio depend heavily on solvent polarity[3,4,7] and pH of the medium.[8,9] Several studies on ESIPT also in micelle,[10,11] proteins,[12,13] and cyclodextrins[14,15] have been reported. It has also been established that not only the electrostatic environment but also the confinement effects strongly influence the ESIPT processes. On the other hand, ESIPT is generally poorly dependent on viscosity since most of the ESIPT dyes are intramolecular hydrogen bonded to form a stable cyclic ring. However, there have been few evidence of strong effect of viscosity on the rate of ESIPT in polar environments.[16] Molecules that exhibiting ESIPT have been very attractive as potential tunable laser dyes, LEDs,[17] photostabilizers,[18] molecular energy storage,[19] high energy radiation detectors,[20] molecular switches,[21] fluorescence probes,[22] and sensors.[23]

SCHEME 1

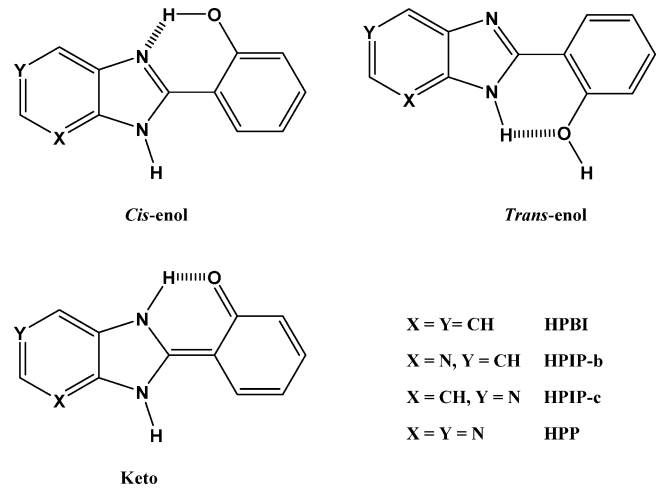

* Corresponding author. Phone: +91-3612582315. Fax: +91-3612582349. E-mail: gkrishna@iitg.ernet.in.

10.1021/jp903535g CCC: $40.75
Published on Web 10/02/2009

SCHEME 2

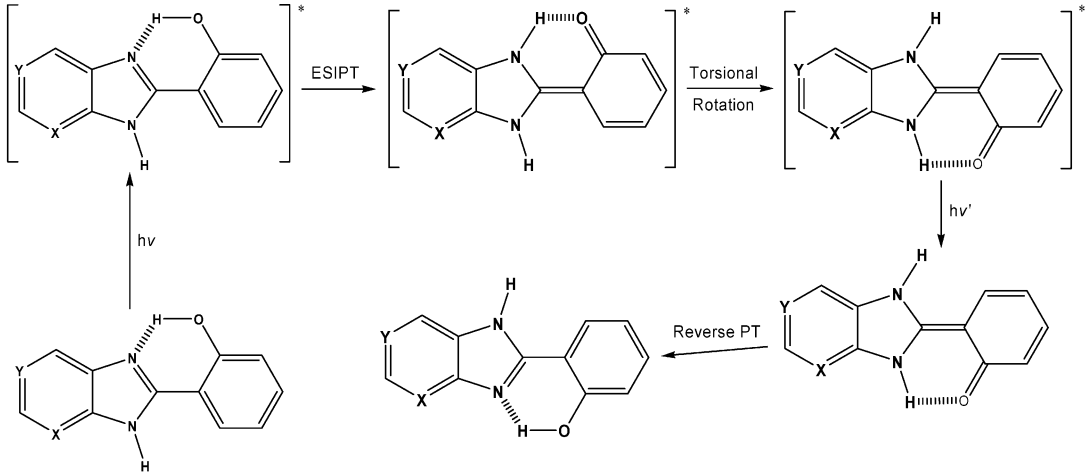

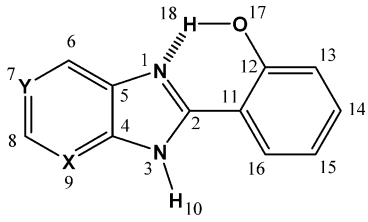

X = N, Y = CH **HPIP-b**
X = CH, Y = N **HPIP-c**
X = Y = N **HPP**

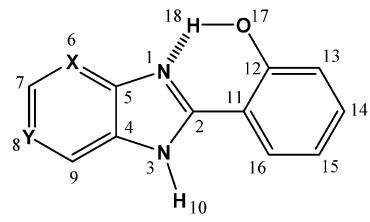

X = N, Y = CH **HPIP-b'**
X = CH, Y = N **HPIP-c'**
X = Y = N **HPP'**

TABLE 1: Relative Energies (eV) of Different Forms of HPIP-b, HPIP-c, HPP, and Their Respective Isomers (HPIP-b′, HPIP-c′, HPP′) with Respect to Their Corresponding *cis*-Enol Forms of HPIP-b, HPIP-c, HPP Isomers in the S_0 State

molecule	*cis*-enol	*trans*-enol	keto
HPIP-b	0.0	0.2526	0.4343
HPIP-b′	0.1497	0.4031	0.5475
HPIP-c	0.0	0.4485	0.2259
HPIP-c′	0.0044	0.2329	0.4365
HPP	0.0	0.2176	0.4700
HPP′	0.1368	0.3560	0.5637

ESIPT in 2-(2′-hydroxyphenyl)benzimidazole (HPBI) had been investigated in detail by several groups.[24−29] The photophysics of 2-(2′-hydroxyphenyl)-3*H*-imidazo[4,5-b]pyridine (HPIP-b) and 2-(2′-hydroxyphenyl)-1*H*-imidazo[4,5-c]pyridine (HPIP-c) were also explored by Dogra et al.[30,31] The common features of HPBI and azo substituted compounds HPIP-b and HPIP-c (Scheme 1) are summarized below: The *cis*-enol, the intramolecularly hydrogen bonded form, is the most stable form of these compounds. Upon excitation, ultrafast intramolecular proton transfer occurs in *cis*-enol form to give phototautomer. In polar/protic solvent *trans*-enol conformer was observed and is responsible for normal emission. But the quantum yields and the excited state lifetimes strongly depend not only on the presence of nitrogen but also on its position.

Several ab initio and semiempirical calculations had been performed on HPBI and other 2-hydroxyphenylbenzazoles to demonstrate the various aspects of their photophysics.[32−36] More recently, Chattopadhyay et al. carried out AM1-SCI calculations on 2-hydroxyphenylbenzazoles including HPBI and compared the calculated results with experimental results.[37,38] Dogra et al. performed semiempirical calculations on HPIP-b and HPIP-c to rationalize the experimental findings.[30,31] But the comparative study on the effect of azo substitution in benzene ring was not examined theoretically. In the present study, we have performed

TABLE 2: Optimized Parameters for Different Enols and Keto Form of Molecules in S_0 and S_1 States[a]

molecule	parameter	*cis*-enol	*trans*-enol	keto
HPBI	ΔE	0.0 (0.0)[b]	0.2597 (0.2621)	0.4075 (−0.3387)
	μ	3.9 (3.8)	4.7 (3.9)	5.9 (4.9)
	R_{OH} (17,18)	0.998 (0.964)	0.970 (0.948)	1.630 (1.963)
	R_{NH} (1,18)	1.732 (1.825)		1.057 (1.001)
	R_{OH} (17,10)		2.038 (2.097)	
HPIP-b	ΔE	0.0 (0.0)	0.2526 (0.3884)	0.4343 (−0.3884)
	μ	1.6 (1.5)	3.6 (2.6)	3.9 (2.7)
	R_{OH} (17,18)	0.996 (0.964)	0.970 (0.948)	1.611 (1.953)
	R_{NH} (1,18)	1.736 (1.824)		1.357 (1.001)
	R_{OH} (17,10)		2.050 (2.112)	
HPIP-b′	ΔE	0.0 (0.0)	0.2534 (0.3574)	0.3979 (−0.4393)
	μ	6.1 (5.8)	6.8 (6.5)	7.4 (6.5)
	R_{OH} (17,18)	0.998 (0.966)	0.970 (0.948)	1.685 (1.987)
	R_{NH} (1,18)	1.735 (1.820)		1.048 (1.001)
	R_{OH} (17,10)		2.030 (2.089)	
HPIP-c	ΔE	0.0 (0.0)	0.2259 (0.3685)	0.4485 (−0.3531)
	μ	5.3 (4.8)	7.3 (5.9)	5.7 (5.1)
	R_{OH} (17,18)	0.996 (0.965)	0.970 (0.948)	1.626 (1.961)
	R_{NH} (1,18)	1.743 (1.821)		1.058 (1.001)
	R_{OH} (17,10)		2.030 (2.102)	
HPIP-c′	ΔE	0.0 (0.0)	0.2286 (0.4001)	0.4321 (−0.3882)
	μ	3.6 (3.9)	6.4 (5.5)	3.5 (2.9)
	R_{OH} (17,18)	0.997 (0.968)	0.970 (0.948)	1.621 (1.954)
	R_{NH} (1,18)	1.737 (1.800)		1.060 (1.954)
	R_{OH} (17,10)		2.029 (2.097)	
HPP	ΔE	0.0 (0.0)	0.2176 (0.2980)	0.4700 (−0.3912)
	μ	3.6 (3.7)	6.5 (5.3)	3.2 (2.9)
	R_{OH} (17,18)	0.995 (0.966)	0.970 (0.948)	1.617 (1.952)
	R_{NH} (1,18)	1.746 (1.816)		1.060 (1.002)
	R_{OH} (17,10)		2.038 (2.117)	
HPP′	ΔE	0.0 (0.0)	0.2193 (0.2946)	0.4270 (−0.4346)
	μ	5.9 (6.4)	8.1 (7.9)	5.7 (5.4)
	R_{OH} (17,18)	0.996 (0.970)	0.970 (0.949)	1.677 (1.973)
	R_{NH} (1,18)	1.741 (1.790)		1.050 (1.002)
	R_{OH} (17,10)		2.022 (2.089)	

[a] Energy difference between other forms and *cis*-enol form (ΔE, eV), dipole moment (μ, D), interatomic distances (R_{xx}, Å). For the atom numbering, refer Scheme 2. Values in parentheses are that correspond to S_1 state. [b] Energy of *cis*-enol in S_0 and S_1 states are −18 672.8614 and −18 672.5751 eV respectively.

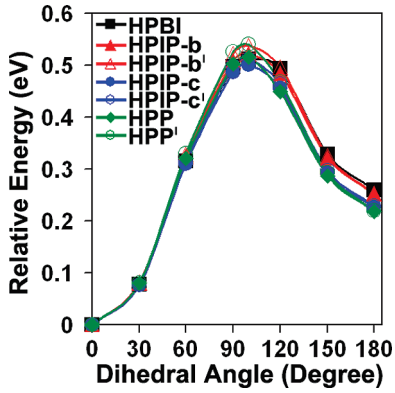

Figure 1. Plot of molecular energy as a function of torsional angle between hydroxyphenyl plane and heterocylic plane for different molecules in S_0 state.

TABLE 3: Calculated Excitation and Fluorescence Spectral Data (nm) for Different Isomers along with Corresponding Experimental Data[a]

	excitation		fluorescence	
	calc	expt	calc	expt
		HPBI		
cis-enol	316	293, 318, 332[b]	341	
trans-enol	307	304, 326[b]	343	360[b,c]
Keto	389		429	458[b,c]
		HPIP-b		
cis-enol	324	318, 327[d]	344	
trans-enol	307	315, 329 (sh)[d]	340	335, 350, 363[d]
Keto	409		450	485[d]
		HPIP-b′		
cis-enol	326		344	
trans-enol	306		337	
Keto	412		451	
		HPIP-c		
cis-enol	315	327[e]	337	
trans-enol	302	299, 309 (sh)[e]	340	337, 342, 355[e]
Keto	392		434	476[e]
		HPIP-c′		
cis-enol	318		336	
trans-enol	293		326	
Keto	395		439	
		HPP		
cis-enol	326		341	
trans-enol	309		339	
Keto	411		456	
		HPP′		
cis-enol	330		344	
trans-enol	317		342	
Keto	416		461	

[a] All experimental data are that of molecule in dioxane. [b] Data from present work. [c] Reference 36. [d] Reference 30. [e] Reference 31.

time dependent density functional theory (TDDFT) calculation on HPBI, HPIP-b, HPIP-c, and 8-(2′-hydroxyphenyl)-9*H*-purine (HPP) to evaluate the effect of nitrogen substitution in the benzene ring on ESIPT and rotamerism. The excitation and emission spectral bands have also been assigned theoretically, and the calculated data agree well with the available experimental literature reports.

2. Methods

All of the calculations in this work were carried out using Gaussian 03W program.[39] The ground state geometries of cis and trans forms of enol and keto form of each compound were obtained by full optimization of structural parameters using DFT employing 6-31G(d) basis set using spin restricted shell wave functions.[40,41] The geometry optimizations were carried out using Becke's three-parameter hybrid functional B3,[42] with nonlocal

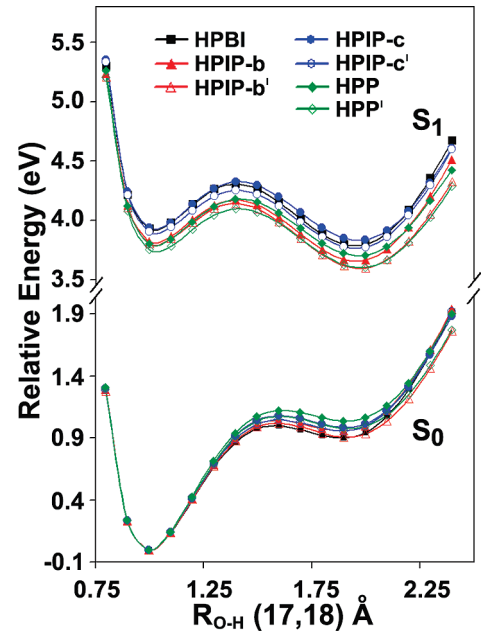

Figure 2. Simulated potential energy surfaces for proton transfer reaction tautomers in the S_1 and S_0 states for different molecules.

TABLE 4: Energy Difference between Keto and *cis*-Enol along the Reaction Coordinates and Barrier for Proton Transfer Reaction (eV)

	energy difference between keto and *cis*-enol	energy barrier	
		cis-enol	keto
	HPBI		
S_1 State	−0.1326	0.3778	0.5104
S_0 State	0.9195	0.9986	0.0790
	HPIP-b		
S_1 State	−0.1557	0.3521	0.5078
S_0 State	0.9535	1.0433	0.0898
	HPIP-b′		
S_1 State	−0.2052	0.3380	0.5431
S_0 State	0.9053	1.0177	0.1124
	HPIP-c		
S_1 State	−0.0985	0.3902	0.4887
S_0 State	0.9851	1.0789	0.0939
	HPIP-c′		
S_1 State	−0.1307	0.3521	0.4829
S_0 State	0.9566	1.0463	0.0897
	HPP		
S_1 State	−0.0972	0.3761	0.4733
S_0 State	1.0357	1.1195	0.0838
	HPP′		
S_1 State	−0.1518	0.3448	0.4966
S_0 State	0.9744	1.0743	0.0999

correlation of Lee−Yang−Parr, LYP,[43] abbreviated as B3LYP. The minimum energy nature of the stationary points was verified from vibrational frequency analysis. Single point calculations were performed with 6-31G+(d,p) basis set on the optimized geometries to obtain the energies. The excitation energies were obtained by vertical excitations of optimized ground states using TDDFT/B3LYP/6-31G+(d,p) calculations.[44,45] The excited state geometries (S_1) were optimized using ab initio restricted configuration interaction singles (RCIS/6-31G(d)) approach.[46] The emission energies were computed by TDDFT/B3LYP/6-31G+(d,p) calculations from the relaxed excited states, that is, using RCIS/6-31G(d) optimized excited state geometries as inputs (vertical transitions).

HPBI was synthesized by literature procedure[24] and purified by column chromatography. AR grade dioxane from Rankem

TABLE 5: Properties of the Energy Minima and the Transition State of Tautomer Rotamers Where the Values in Parentheses Are That of Ab Initio Calculations[a]

	cis-keto	twisted-keto	*trans*-keto
	HPBI		
relative energy (eV)	0.0	−0.2619 (0.3769)	
$S_1 \rightarrow S_0$ transition energy (eV)	2.89 (3.93)	0.75 (2.19)	
oscillator Strength	0.3300 (0.6100)	0.0001 (0.0010)	
	dipole moment (D)		
S_1 state	(4.9)	(3.6)	
S_0 state	5.9	8.2	
	charge on benzimidazole ring		
S_1 state	(0.5423)	(0.0816)	
S_0 state	0.8496	(0.6536)	
	charge on phenolic moiety		
S_1 state	(−0.5423)	(−0.0816)	
S_0 state	−0.8496	(−0.6536)	
ϕ_f	0.65 (ref 24)		
	HPIP-b		
relative energy (eV)	0.0	−0.2589 (0.3391)	0.0870 (0.0704)
$S_1 \rightarrow S_0$ transition energy (eV)	2.76 (3.88)	0.70 (2.21)	2.75 (3.86)
oscillator strength	0.3024 (0.6324)	0.0003 (0.0011)	0.3122 (0.6438)
	dipole moment (D)		
S_1 state	(2.7)	(4.3)	(6.5)
S_0 state	3.9	7.6	7.4
	charge on imidazopyridine ring		
S_1 state	(0.3754)	(0.0763)	(0.3759)
S_0 state	0.8895	(0.6808)	0.9173
	charge on phenolic moiety		
S_1 state	(−0.3754)	(−0.0763)	(−0.3759)
S_0 state	−0.8895	(−0.6808)	−0.9173
ϕ_f	0.26 (ref 30)		
	HPIP-c		
relative energy (eV)	0.0	−0.3422 (0.2711)	−0.0355 (−0.0194)
$S_1 \rightarrow S_0$ transition energy (eV)	2.85 (3.91)	0.67 (2.12)	2.83 (3.90)
oscillator strength	0.2941 (0.5591)	0.0001 (0.0006)	0.2891 (0.5684)
	dipole moment (D)		
S_1 state	(5.1)	(6.2)	(2.9)
S_0 state	5.7	6.2	3.5
	charge on imidazopyridine ring		
S_1 state	(0.3780)	(0.0734)	(0.2343)
S_0 state	0.3711	(0.6430)	0.3701
	charge on phenolic moiety		
S_1 state	(−0.3780)	(−0.0734)	(−0.2343)
S_0 state	−0.3711	(−0.6430)	−0.3701
ϕ_f	0.22 (ref 31)		
	HPP		
relative energy (eV)	0.0	−0.3437 (0.2124)	0.0544 (0.0470)
$S_1 \rightarrow S_0$ transition energy (eV)	2.72 (3.85)	0.57 (2.09)	2.69 (3.82)
oscillator strength	0.2684 (0.5689)	0.0002 (0.0006)	0.2761 (0.5912)
	dipole moment (D)		
S_1 state	(2.9)	(6.6)	(5.4)
S_0 state	3.2	5.3	5.7
	charge on Purine ring		
S_1 state	(0.3469)	(0.0642)	(0.3431)
S_0 state	0.7933	(0.5019)	0.7972
	charge on phenolic moiety		
S_1 state	(−0.3469)	(−0.0642)	(−0.3431)
S_0 state	−0.7933	(−0.5019)	−0.7972

[a] Fluorescence quantum yields (ϕ_f) are that of tautomers in dioxane.

India was used as received. Fluorescence emission and excitation spectra were recorded using Edinburgh Instrument FSP 920 steady state fluorimeter.

3. Results and Discussion

3.1. Molecular Geometries and Energies. Two isomeric forms are possible for HPIP-b, HPIP-c, and HPP, and we labeled respective isomeric forms as HPIP-b′, HPIP-c′, and HPP′ (Scheme 2). The optimized energies calculated for all of the forms of both isomers are compared in Table 1. For all rotameric and tautomeric forms, HPIP-b, HPIP-c, and HPP isomers are more stable than their respective forms of HPIP-b′, HPIP-c′, and HPP′ isomers. The keto forms of the isomers are interconvertable by torsional rotation of phenolic moiety. Torsional rotation of keto form followed by reverse proton transfer will lead to other isomers (Scheme 2).

The optimized parameters of *cis*-enol, *trans*-enol, and keto forms for all of the molecules in the ground state are compiled in Table 2. The calculation predicts the *cis*-enol as the most stable geometry in all of the molecules and further predicts the

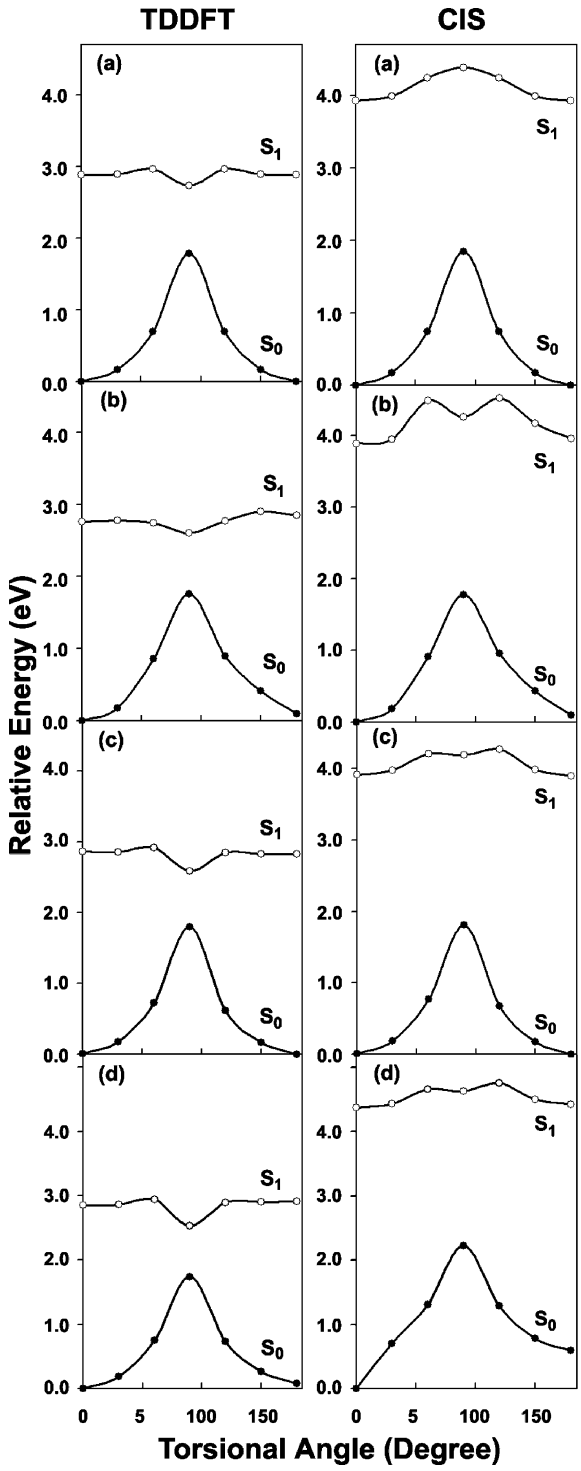

Figure 3. Simulated potential energy surfaces for torsion rotation of tautomers in the S_1 and S_0 states (a) HPBI, (b) HPIP-b, (c) HPIP-c, and (d) HPP (left panel TDDFT calculations and right panel CIS calculations).

dihedral angles between the imidazole ring and the phenyl ring to be 0° and 180° in *cis*- and *trans*-enol conformers in all molecules. The corresponding angles reported from semiempirical calculations for HPBI,[36,37] HPIP-b,[30] and HPIP-c[31] are about 40° and 140°. The relative stability of the *cis*-enol to *trans*-enol decreases with nitrogen substitution and follows the order HPBI > HPIP-b′ > HPIP-b > HPIP-c′ > HPIP-c > HPP′ > HPP. This may be due to relative weakening of hydrogen bond between N_1 and H_{18} in cis conformer of enol (Table 2). Thus substitution of nitrogen in benzene ring affects the relative population of the two rotamers in the ground state. The potential energy surfaces for conversion of *cis*-enol to *trans*-enol are constructed by optimizing the molecular geometries with different preset torsional angle between the hydroxyphenyl plane and the heterocylic plane. The potential energy surfaces thus constructed are shown in Figure 1. The barrier height for the conversion of *cis*-enols to *trans*-enols are found to be 0.512, 0.522, 0.538, 0.501, 0.511, 0.515, and 0.541 eV for HPBI, HPIP-b, HPIP-b′, HPIP-c, HPIP-c′, HPP, and HPP′ respectively. The barrier heights for the reverse transformation for the compounds are 0.252, 0.270, 0.285, 0.275, 0.283, 0.297, and 0.322 eV respectively.

On the other hand the relative stability of *cis*-enol to keto tautomer increases in the order HPIP-b′ < HPBI < HPP′ < HPIP-c′ < HPIP-b < HPIP-c < HPP. In general, the relative stability of *cis*-enol to keto tautomer increases with nitrogen substitution. Exceptional behavior of HPIP-b′ and HPP′ may be due to the presence of pyridine ring nitrogen (N_6) with lone pair near the imidazole nitrogen (N_1) that has the lone pair and the proton transfer reduce the lone pair−lone pair repulsion.

Since the experimental excitation energies are available in literature for both the conformers (except for HPP), we calculated and compared the excitation energy of different forms with the experimental values (Table 3). The calculated data show that the excitation spectrum was red-shifted on moving from HPBI to HPIP-c to HPIP-b and is consistent with the experimental report. The excitation energies predicted by the calculations are also in reasonable agreement with experimental data.

The parameters obtained for optimized molecular geometries in the first excited state are compiled in Table 2. The energy difference between the *cis*-enol and the keto increases with nitrogen substitution. The fluorescence data calculated for different isomers are in reasonable agreement with the available experimental spectral data (Table 3).

3.2. Proton Transfer. The CIS method is known to overestimate the energy barriers for proton transfer reactions.[35,47,48] The TDDFT has been proven much more reliable with proton transfer reactions.[35,47−50] Thus, the potential energy surface for proton transfer process has been generated in S_0 and S_1 states using the distinguished coordinate approach with the OH bond elongation as the primary reaction coordinate by TDDFT/B3LYP/6-31G+(d,p) calculations. The diagrams are shown in Figure 2, and the data are compiled in Table 4. The general features of potential energy surfaces are summarized below. The proton transfer process is endothermic in the ground state and exothermic in the first excited state. Thus, thermodynamically unfavorable proton transfer process becomes thermodynamically favorable in S_1 state. The potential energy barrier for the proton transfer reaction also appreciably lowered in the S_1 state compared with that in the S_0 state and became favored in the S_1 state compared with that in the ground state. The barrier for reverse transfer is very small in the S_0 state but increases in the S_1 state. The energy difference between the enol and the keto tautomers along the reaction coordinates in S_0 state increase in the order HPIP-b′ < HPBI < HPIP-b < HPIP-c′ < HPP′ < HPIP-c < HPP. On the other hand, that in S_1 state, that is, the thermodynamic feasibility of the proton transfer in the S_1 state, decreases with nitrogen substitution except HPIP-b, HPIP-b′, and HPP′. Similar effect was also found when −NH− is replaced by more electronegative −S− and −O− in HPBI.[34] The difference in behavior of HPIP-b′ and HPP′ may be due to the reduced lone pair−lone pair repulsion in keto tautomer as mentioned earlier. This was further supported by the fact that the barrier height for reverse proton transfer follows the order

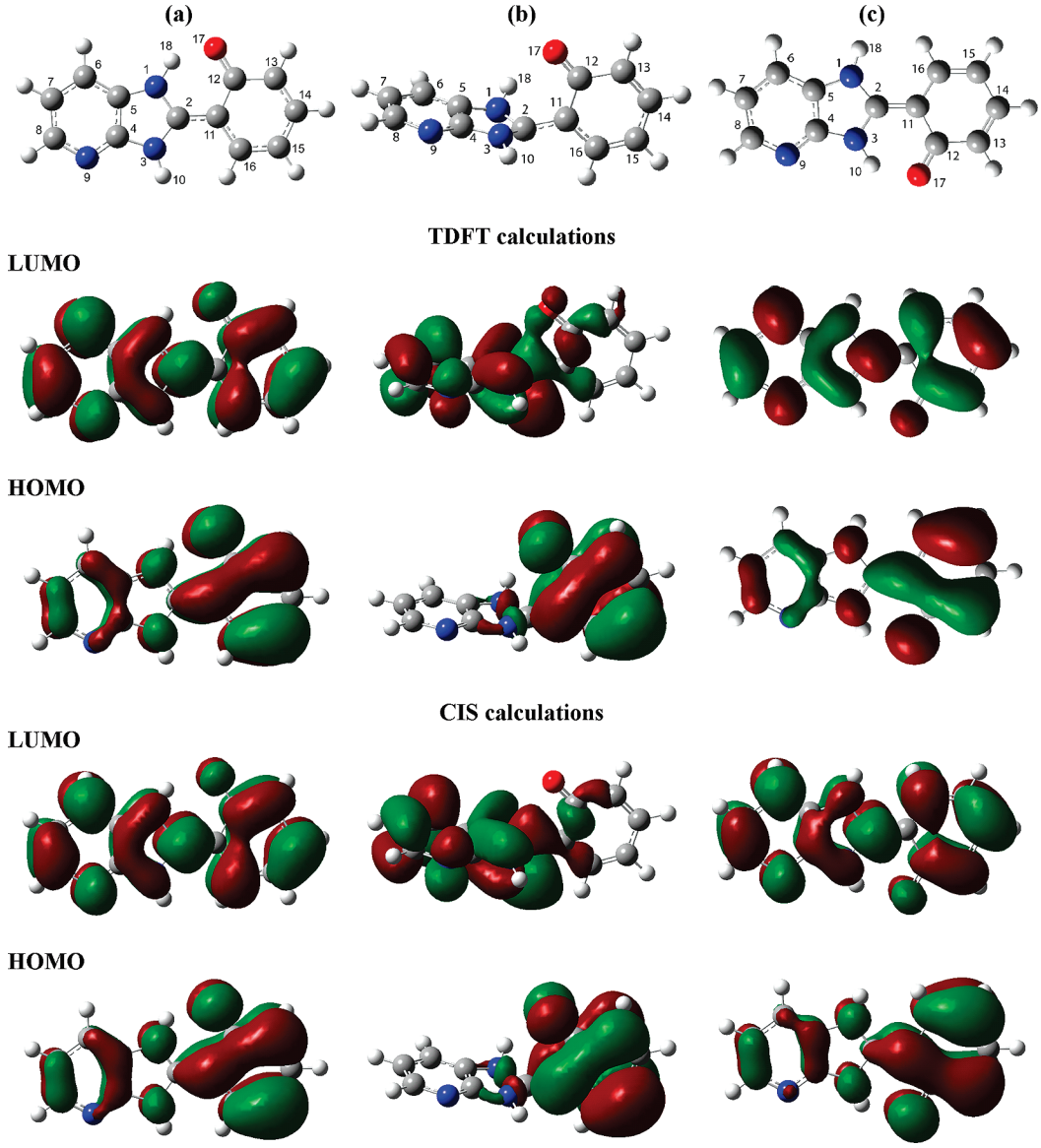

Figure 4. Optimized structures of (a) *cis*, (b) twisted minimum, and (c) *trans* of keto on the excited state surface along with corresponding LUMO (upper) and HOMO (lower) for HPIP-b. Similar results have been determined for other molecules (Supporting Information).

HPIP-b′ > HPBI > HPIP-b > HPP′ > HPIP-c > HPIP-c′ > HPP; that is, HPIP-b′ is higher than HPBI and HPP′ is higher than HPIP-c′.

3.3. Torsional Rotation of Keto Tautomer. One of the important consequences of nitrogen substitution is the decrease in the fluorescence quantum yield (Table 5). Several mechanisms for nonradiative transition of ESIPT molecules have been proposed but still unproven. The intramolecular charge transfer (ICT) reaction in the excited state keto form which result in twisted geometry is proposed as one of the possible path for quenching in 2-(2′-hydroxyphenyl)-oxazole (HPO) and thiazole (HPT).[52] Ab initio calculations on HPO and HPT predicted twisted conformations that have a biradicaloid nature and have the minimum energy in the S_1 state. Vazquez et al. investigated the effect of substituting nitrogen on the phenyl ring of 2-(2′-hydroxyphenyl)benzazoles and suggested that the radiationless decay involves a proton coupled charge transfer process from dissociated phenol or pyridinol moiety to protonated benzazole moiety.[53] With dissociated phenol being a better donor than the dissociated pyridinol moiety, with increase in electron accepting strength by nitrogen substitution in protonated benzimidazole, the feasibility of such a process increases in the present systems.

We have constructed the potential energy surface for torsional motion of hydroxyphenyl moiety relative to the heterocylic ring from the relaxed keto tautomers by performing partial optimization on different geometries that have preset torsional angle. As mentioned earlier, such a rotational motion of HPIP-b, HPIP-c, and HPP keto tautomers results in the respective keto tautomers obtained from HPIP-b′, HPIP-c′, and HPP′. Then, as in other cases, we have performed single point TDDFT calculations over CIS optimized geometries. From these calculations, it is found that the first electronic transition ($S_1 \leftarrow S_0$) corresponded only to the promotion of an electron from HOMO to LUMO in all of these molecules. The potential energy surfaces constructed by TDDFT predict that cis and trans rotamers are stable forms of keto tautomer in S_0 as well as in S_1 states (Figure 3). The perpendicular geometry of tautomer possesses the maximum energy in S_0 state and the minimum energy in S_1 state. The full optimization of S_1 minimum starting with the perpendicular structure of the S_0 state leads to a bent or twisted structure with nonplanar heterocyclic subsystems (Figure 4 and Table 6). This twisted structure is the result of pyramidalization of imidazole ring subsystem by rehybridization. Such a rehybridization is due to increase in electron density of

TABLE 6: Selected Bond Lengths and Angles of the Keto Tautomers in the Optimized S_0 and S_1 States[a]

	cis-keto		twisted-keto		*trans*-keto	
geometry parameters	S_0 state	S_1 state	S_0 state	S_1 state	S_0 state	S_1 state
			HPBI			
N1 C2	1.353	1.358	1.350	1.409		
N3 C2	1.370	1.370	1.350	1.410		
C2 C11	1.416	1.406	1.448	1.436		
C11 C12	1.463	1.502	1.461	1.488		
C11 C16	1.420	1.394	1.407	1.421		
C12 O17	1.273	1.230	1.258	1.207		
N1 C2 C11 C12	0.00	−0.10	88.0	67.7		
C5 N1 C2 C11	180.0	180.0	−174.93	−151.8		
			HPIP-b			
N1 C2	1.358	1.360	1.354	1.411	1.376	1.371
N3 C2	1.371	1.371	1.350	1.402	1.356	1.360
C2 C11	1.414	1.406	1.446	1.438	1.410	1.407
C11 C12	1.463	1.499	1.462	1.488	1.466	1.499
C11 C16	1.421	1.392	1.407	1.419	1.423	1.392
C12 O17	1.274	1.231	1.258	1.207	1.267	1.229
N1 C2 C11 C12	0.1	0.0	88.4	67.9	180.0	180.0
C5 N1 C2 C11	179.8	180.0	−174.4	−149.1	180.0	180.0
			HPIP-c			
N1 C2	1.353	1.357	1.349	1.410	1.370	1.368
N3 C2	1.376	1.376	1.355	1.410	1.359	1.364
C2 C11	1.413	1.406	1.445	1.435	1.413	1.406
C11 C12	1.464	1.501	1.462	1.488	1.464	1.501
C11 C16	1.421	1.391	1.407	1.421	1.422	1.391
C12 O17	1.272	1.230	1.258	1.207	1.272	1.230
N1 C2 C11 C12	−0.02	−0.01	87.6	68.1	180.0	180.0
C5 N1 C2 C11	180.0	180.0	−174.5	−151.7	180.0	180.0
			HPP			
N1 C2	1.358	1.359	1.353	1.412	1.376	1.370
N3 C2	1.378	1.377	1.356	1.404	1.363	1.365
C2 C11	1.409	1.406	1.443	1.436	1.406	1.407
C11 C12	1.465	1.498	1.462	1.488	1.468	1.498
C11 C16	1.423	1.390	1.408	1.419	1.389	1.425
C12 O17	1.271	1.230	1.258	1.207	1.266	1.229
N1 C2 C11 C12	0.0	0.0	87.9	69.3	180.0	180.0
C5 N1 C2 C11	180.0	180.0	−174.0	−149.5	180.0	180.0

[a] For the atom numbering, refer Figure 4.

five member ring and is consistent with the literature report.[51,53] The charge calculations on heterocylic and phenolic moieties indicate the dot−dot electronic configuration for the perpendicular geometry in the S_1 state. The dot−dot electronic configuration is consistent with previous finding of HPO and HPT.[51] However, it was reported for HPO and HPT that the $S_1 \rightarrow S_0$ transition corresponds to the transfer of nearly full electron. In the present cases, the charges on the individual moieties in the ground state suggests that $S_1 \rightarrow S_0$ transition corresponds to partial electron transfer from heterocylic moiety to phenolic moiety.

It is reported in the literature that TDDFT poorly describes some charge transfer situations, in which there is little or no overlap between the atomic orbitals contributing to the HOMO and those contributing to the LUMO.[54,55] Since we have also constructed the potential energy surface by performing single point over CIS optimized geometries, we have presented the CIS energy curves also (Figure 3). CIS curve for HPBI differs significantly from that of TDDFT in the sense that, unlike TDDFT, no minimum is observed at the twisted geometry by CIS. Similarly, a barrier was found at twisted keto for 2-(2′-hydroxyphenyl)-4-methyloxazole by CIS calculation.[50] On the other hand, in nitrogen substituted analogues, CIS also predicted a minimum for twisted geometry. But, the energies of the twisted geometries are higher than that of planar isomers. While the transition energies calculated for planar keto by TDDFT is closer to experimental values, the CIS method overestimates them. It is difficult to predict that the TDDFT or CIS is closer to the correct description. A search was also done for the possible conical intersection (CI) in the region using complete active space self-consistent field (CASSCF) calculations. The calculations were performed by employing 6-31G basis set with an active space of (2, 2) involving two electrons and two oribitals. But, CASSCF calculations do not indicate any crossing of S_1 and S_0 states in any of the molecule. The energy differences obtained by these calculations for HPBI, HPIP-b, HPIP-c, and HPP are 1.02, 0.96, 0.89, and 0.88 eV, respectively, and are closer to values obtained by TDDFT than CIS calculations. However, all of the calculations predict that the S_1-S_0 energy gap decreases in order HPBI > HPIP-b > HPIP-c > HPP (Table 5). According to energy gap law, the decrease in energy gap would lead to increase in nonradiative rate. Thus, the nitrogen substitution in benzene ring of HPBI increases the torsion induced nonradiative decay of keto tautomer in the order HPBI < HPIP-b < HPIP-c < HPP. The results are in good agreement with the experimental findings that the fluorescence quantum yield for tautomer decreases in the order HPBI > HPIP-b > HPIP-c.[30,31]

4. Conclusion

A comparative theoretical study of nitrogen substitution in the benzene ring of HPBI is presented. The calculated excitation and fluorescence spectral data agree well with the available

experimental results. The present study also reveals that (i) all molecules have two stable rotameric forms in the ground state, and the relative stability of *cis*-enol decreases with nitrogen substitution. (ii) For all of the molecules, the intramolecular proton transfer is unfavorable in the S_0 state and becomes feasible in the S_1 state. (iii) The energy difference between the keto and the enol forms along the proton transfer coordinates in the S_1 state decreases in the order HPIP-b′ > HPIP-b > HPP′ > HPBI > HPIP-c′ > HPIP-c > HPP. (iv) Torsion rotation of the tautomer to form twisted structure is one of the nonradiative channels for the tautomer. At this conformation, the S_1-S_0 energy gap is reduced in order HPBI > HPIP-b > HPIP-c > HPP. (v) The influence of nitrogen substitution on photophysics of HPBI depends not only on the number of nitrogen atom present in the benzene ring but also on the position of nitrogen atom.

Acknowledgment. We are grateful to the reviewers for their suggestion in the interpretation about the significance of twisted geometry. The work is supported by Department of Science and Technology, New Delhi through funding the project SR/S1/PC-19/2006. F.A.S.C. acknowledges CSIR, New Delhi for the Junior Research Fellowship.

Supporting Information Available: Optimized structures of *cis*, twisted minimum, and *trans* of tautomer on the excited state surface along with corresponding LUMO and HOMO for HPBI, HPIP-c, and HPP. This material is available free of charge via the Internet at http://pubs.acs.org.

References and Notes

(1) Kasha, M. *J. Chem. Soc., Faraday Trans. 2* **1986**, *82*, 2379–2392.
(2) Douhal, A.; Kim, S. K.; Zewail, A. H. *Nature* **1995**, *378*, 260–263.
(3) Chen, C.-L.; Lin, C.-W.; Hsieh, C.-C.; Lai, C.-H.; Lee, G.-H.; Wang, C.-C.; Chou, P.-T. *J. Phys. Chem. A* **2009**, *113*, 205–214.
(4) Lukeman, M.; Wan, P. *J. Am. Chem. Soc.* **2002**, *124*, 9458–9464.
(5) Frey, W.; Elsaesser, T. *Chem. Phys. Lett.* **1992**, *189*, 565–570.
(6) Schwartz, B. J.; Peteanu, L. A.; Harris, C. B. *J. Phys. Chem.* **1992**, *96*, 3591–3598.
(7) Seo, J.; Kim, S.; Park, S. Y. *J. Am. Chem. Soc.* **2004**, *126*, 11154–11155.
(8) Santra, S.; Krishnamoorthy, G.; Dogra, S. K. *Chem. Phys. Lett.* **2000**, *327*, 230–237.
(9) Prieto, F. R.; Mosquera, M.; Novo, M. *J. Phys. Chem.* **1990**, *94*, 8536–8542.
(10) Das, S. K.; Dogra, S. K. *Bull. Chem. Soc. Jpn.* **1997**, *70*, 307–313.
(11) Sarkar, N.; Das, K.; Das, S.; Datta, A.; Nath, D.; Bhattacharyya, K. *J. Phys. Chem.* **1995**, *99*, 17711–17714.
(12) Sytnik, A.; Kasha, M. *Proc. Natl. Acad. Sci. U.S.A.* **1994**, *91*, 8627–8630.
(13) Maity, S. S.; Samanta, S.; Sardar, P. S.; Pal, A.; Dasgupta, S.; Ghosh, S. *Chem. Phys.* **2008**, *354*, 162–173.
(14) Douhal, A. *Chem. Rev.* **2004**, *104*, 1955–1976.
(15) Roberts, E. L.; Dey, J.; Warner, I. M. *J. Phys. Chem. A* **1997**, *101*, 5296–5301.
(16) Yushchenko, D. A.; Shvadchak, V. V.; Klymchenko, A. S.; Duportail, G.; Pivovarenko, V. G.; Mély, Y. *J. Phys. Chem. A* **2007**, *111*, 10435–10438.
(17) Chou, P.; McMorrow, D.; Aartsma, T. J.; Kasha, M. *J. Phys. Chem.* **1984**, *88*, 4596–4599.
(18) Paterson, M. J.; Robb, M. A.; Blancafort, L.; DeBellis, A. D. *J. Phys. Chem. A* **2005**, *109*, 7527–7537.
(19) Nishiya, T.; Yamuchi, S.; Hirota, N.; Baba, M.; Hamazaki, I. *J. Phys. Chem.* **1986**, *90*, 5730–5735.
(20) Chou, P. T.; Martinej, M. L. *Radiat. Phys. Chem.* **1993**, *41*, 373–378.
(21) Zhang, G.; Wang, H.; Yu, Y.; Xiong, F.; Tang, G.; Chen, W. *Appl. Phys. B: Lasers and Opt.* **2003**, *76*, 677–681.
(22) Ozturk, T.; Klymchenko, A. S.; Capan, A.; Oncul, S.; Cikrikci, S.; Taskiran, S.; Tasan, B.; Kaynak, F. B.; Ozbey, S.; Demchenko, A. P. *Tetrahedron* **2007**, *63*, 10290–10299.
(23) Wu, Y.; Peng, X.; Fan, J.; Gao, S.; Tian, M.; Zhao, J.; Sun, S. *J. Org. Chem.* **2007**, *72*, 62–70.
(24) Sinha, H. K.; Dogra, S. K. *Chem. Phys.* **1986**, *102*, 337–347.
(25) Waluk, J. In *Conformational Analysis of Molecules in Excited States*; Waluk, J., Ed.; Wiley-VCH: New York, 2000; Chapter *2*.
(26) Douhal, A.; Amat-Guerrib, F.; Lillo, M. P.; Acuña, A. W. *J. Photochem. Photobiol. A* **1994**, *78*, 127–138.
(27) Itoh, M.; Fujiwara, Y. *J. Am. Chem. Soc.* **1985**, *107*, 1561–1565.
(28) Dupradeau, F. Y.; Case, D. A.; Yu, C. Z.; Jimenez, R.; Romesberg, F. E. *J. Am. Chem. Soc.* **2005**, *127*, 15612–15617.
(29) Rini, M.; Kummrov, A.; Dreyer, J.; Nibbering, E. T. J.; Elsaesser, T. *Faraday Discuss.* **2003**, *122*, 27–40.
(30) Krishnamoorthy, G.; Dogra, S. K. *J. Lumin.* **2001**, *92*, 91–102.
(31) Balamurali, M. M.; Dogra, S. K. *J. Photochem. Photobiol. A* **2002**, *154*, 81–92.
(32) Das, K.; Sarkar, N.; Majumdar, D.; Bhattacharyya, K. *Chem. Phys. Lett.* **1992**, *198*, 443–448.
(33) Forés, M.; Duran, M.; Adamowicz, L. *J. Phys. Chem. A* **1999**, *103*, 4413–4420.
(34) Ríos, M. A.; Ríos, M. C. *J. Phys. Chem. A* **1998**, *102*, 1560–1567.
(35) de Vivie-Riedle, R.; De Waele, V.; Kurtz, L.; Riedle, E. *J. Phys. Chem. A* **1999**, *103*, 10591–10599.
(36) Das, K.; Sakar, N.; Ghosh, A. K.; Majumdar, D.; Nath, D. N.; Bhattacharyya, K. *J. Phys. Chem.* **1994**, *98*, 9126–9132.
(37) Purkayastha, P.; Chattopadhyay, N. *Phys. Chem. Chem. Phys.* **2000**, *2*, 203–210.
(38) Purkayastha, P.; Chattopadhyay, N. *Int. J. Mol. Sci* **2003**, *4*, 335–361.
(39) Frisch, M. J.; Trucks, G. W.; Schlegel, H. B.; Scuseria, G. E.; Robb, M. A.; Cheeseman, J. R.; Montgomery, J. A.; Jr., Vreven; T. Kudin, K. N.; Burant, J. C.; Millam, J. M.; Iyengar, S. S.; Tomasi, J.; Barone, V.; Mennucci, B.; Cossi, M.; Scalmani, G.; Rega, N.; Petersson, G. A.; Nakatsuji, H.; Hada, M.; Ehara, M.; Toyota, K.; Fukuda, R.; Hasegawa, J.; Ishida, M.; Nakajima, T.; Honda, Y.; Kitao, O.; Nakai, H.; Klene, M.; Li, X.; Knox, J. E.; Hratchian, H. P.; Cross, J. B.; Bakken, V.; Adamo, C.; Jaramillo, J.; Gomperts, R.; Stratmann, R. E.; Yazyev, O.; Austin, A. J.; Cammi, R.; Pomelli, C.; Ochterski, J. W.; Ayala, P. Y.; Morokuma, K.; Voth, G. A.; Salvador, P.; Dannenberg, J. J.; Zakrzewski, V. G.; Dapprich, S.; Daniels, A. D.; Strain, M. C.; Farkas, O.; Malick, D. K.; Rabuck, A. D.; Raghavachari, K.; Foresman, J. B.; Ortiz, J. V.; Cui, Q.; Baboul, A. G.; Clifford, S.; Cioslowski, J.; Stefanov, B. B.; Liu, G.; Liashenko, A.; Piskorz, P.; Komaromi, I.; Martin, R. L.; Fox, D. J.; Keith, T.; Al-Laham, M. A.; Peng, C. Y.; Nanayakkara, A.; Challacombe, M.; Gill, P. M. W.; Johnson, B.; Chen, W.; Wong, M. W.; Gonzalez, C.; Pople, J. A. *Gaussian 03, Revision E.01*; Gaussian, Inc.: Wallingford, CT, 2004.
(40) Hohenberg, P.; Kohn, W. *Phys. Rev. B* **1964**, *136*, 864–871.
(41) Kohn, W.; Sham, L. J. *Phys. Rev. A* **1965**, *140*, 1133–1138.
(42) Becke, A. D. *J. Chem. Phys.* **1993**, *98*, 5648–5652.
(43) Lee, C.; Yang, W.; Parr, R. G. *Phys. Rev. B* **1988**, *37*, 785–789.
(44) Casida, M. E. In *Recent Advances in Density Functional Methods, Part I*; Chong, D. P., Ed.; World Scientific: Singapore, 1995; p 155.
(45) Gross, E.; Dobson, J.; Petersilka, M. *Top. Curr. Chem.* **1996**, *181*, 81–172.
(46) Foresman, J. B.; Head-Gordon, M.; Pople, J. A.; Frisch, M. J. *J. Phys. Chem.* **1992**, *96*, 135–149.
(47) Vendrell, O.; Moreno, M.; Lluch, J. M. *J. Chem. Phys.* **2002**, *117*, 7525–7533.
(48) Casadesús, R.; Vendrell, O.; Moreno, M.; Lluch, J. M. *Chem. Phys. Lett.* **2005**, *405*, 187–192.
(49) Vendrell, O.; Gelabert, R.; Moreno, M.; Lluch, J. M. *Chem. Phys. Lett.* **2004**, *396*, 202–207.
(50) Casadesús, R.; Moreno, M.; Lluch, J. M. *J. Photochem. Photobiol. A* **2005**, *173*, 365–374.
(51) LeGourriérec, D.; Kharlanov, V.; Brown, R. G.; Rettig, W. *J. Photochem. Photobiol. A* **2000**, *130*, 101–111.
(52) Vázquez, S. R.; Rodríguez, C. R.; Mosquera, M.; -Prieto, F. R. *J. Phys. Chem. A* **2007**, *111*, 1814–1826.
(53) Kharlanov, V. A.; Rettig, W.; Knyazhansky, M. I.; Makaraova *J. Photochem. Photobiol. A* **1997**, *103*, 45–50.
(54) Dreuw, A.; Weisman, J. L.; Head-Gordon, M. *J. Chem. Phys.* **2003**, *119*, 2943–2946.
(55) Sobolewski, A. L.; Domcke, W. *Chem. Phys.* **2003**, *294*, 73–83.

JP903535G